FARADAY

Effect of block architecture on the micellisation and gelation of block copolymers of ethylene oxide and 1,2-butylene oxide in aqueous solution

Antonis Kelarakis,[a] Vasiliki Havredaki,[a] Leo Derici,[b] Ga-Er Yu,[b] Colin Booth*[b] and Ian W. Hamley[c]

[a] *National and Kapodistrian University of Athens, Department of Chemistry, Physical Chemistry Laboratory, Panepistimiopolis, 157 71 Athens, Greece*
[b] *Manchester Polymer Centre, Department of Chemistry, University of Manchester, Manchester, UK M13 9PL*
[c] *School of Chemistry, University of Leeds, Leeds, UK LS2 9JT*

Received 24th September 1998, Accepted 21st October 1998

Block copolymers $E_{106}B_{16}$, $E_{210}B_{16}$ and $E_{103}B_{15}E_{103}$ (E = oxyethylene, B = oxybutylene) were synthesised and characterised by gel permeation chromatography (for molar mass distribution) and ^{13}C NMR spectroscopy (for number-average molar mass and composition). Surface tensiometry was used to determine critical micelle concentrations at several temperatures, and thereby values of the enthalpy of micellisation. In the case of the diblock copolymers the micellisation was athermal. Dynamic and static light scattering were used to characterise the micelles in solution, yielding micellar association number, hydrodynamic and thermodynamic radius, and the related thermodynamic expansion factor. The latter was used to correlate the dilute solution properties of the copolymer micelles with their critical gelation concentrations. The gels were studied by small-angle X-ray scattering (SAXS) in tandem with rheology (oscillatory shear). Values of the elastic dynamic modulus (G') of the gels significantly exceeded 10^4 Pa across the range of temperatures (25–75 °C) and frequency (0.1–100 rad s^{-1}) explored, allowing the gels to be characterised as 'hard'. SAXS, whether from unoriented or shear-oriented gels, showed them to comprise structures with body-centred cubic (bcc, space group $Im\bar{3}m$) symmetry. In particular, the patterns from the sheared gels were indexed to a highly twinned structure in which a [111] direction of the bcc lattice lay along the shear direction, and flow was mainly in the {211} plane for $E_{103}B_{15}E_{103}$ gels, but in the intersecting {110}, {211} and {321} planes for the diblock copolymer gels. For one copolymer, $E_{106}B_{16}$, micellar radii (calculated assuming sphericity) and association numbers in the gel were obtained. Compared with equilibrium (thermodynamic) values in dilute solution, the micellar radii were similar but the micellar association number in the gel was larger.

1 Introduction

Water soluble block copolyethers of suitable composition micellise in solution and their concentrated micellar solutions form liquid-crystal mesophases (gels). Investigations of the properties of $E_mP_nE_m$ triblock copolymers [E denotes an oxyethylene unit, OCH_2CH_2, and P an oxypropylene unit, $OCH_2CH(CH_3)$] were first reported in the mid-1950s, and the literature has expanded greatly since the mid-1960s. From a physico-chemical viewpoint, interest lies in the characteristics of the micelles themselves and in the structures of the mesophases formed therefrom. Excellent reviews summarise early[1] and recent[2,3] work.

Block copolymers of ethylene oxide and 1,2-butylene oxide have recently become available from The Dow Chemical Company, Freeport, Texas in both diblock and triblock form.[4,5] These materials were first described some years ago,[1] but systematic studies of their self-association properties were not undertaken until the early 1990s, as recently reviewed.[6] E/B block copolymers [B = oxybutylene, $OCH_2CH(C_2H_5)$] have certain advantages over E/P block copolymers in detailed studies of association properties, not least because the hydrophobicity of a B unit is higher than that of a P unit.[7–9] This promotes micellisation in dilute aqueous solution of copolymers with relatively short block lengths. A second important factor is the ease of preparation of E/B copolymers by sequential anionic polymerisation. The transfer reaction, which complicates the anionic polymerisation of propylene oxide,[10] is insignificant in the anionic polymerisation of 1,2-butylene oxide under laboratory conditions. Consequently, the molar mass distributions of diblock copolymers (E_mB_n) and triblock copolymers ($B_nE_mB_n$) are usually very narrow, *i.e.* ratios of mass-to-number-average molar mass, M_w/M_n, below 1.05. The slow rate of reaction of ethylene oxide with the secondary oxyanions of a first-formed B block leads to somewhat wider molar mass distributions for $E_mB_nE_m$ copolymers.[11,12]

Direct comparisons of the association properties of E_mB_n and $E_{m/2}B_nE_{m/2}$ copolymers have been made for copolymers with rather short E ($m \approx 40$) and B blocks ($n \approx 8$ or 12).[7,13–15] The work reported in this paper extends the range of comparison within the E/B system to copolymers with significantly longer E-block lengths, specifically to $E_{210}B_{16}$ and $E_{103}B_{15}E_{103}$, together with the closely related copolymer $E_{106}B_{16}$.

Recently, these copolymers have formed a basis for a number of reports: (i) the effect of block architecture on the adsorption of the copolymers onto polystyrene latex, studied by small-angle neutron scattering (SANS);[16] (ii) the crystallography of the body-centred cubic mesophase of copolymer $E_{210}B_{16}$ by SANS;[17] (iii) the thermodynamics of micellisation

of the diblock copolymers *via* determination of their critical micelle concentrations by surface tensiometry.[18] However, a full account of their association behaviour, including both micellisation and gelation, has not been published. This account goes some way towards meeting that need.

2 Experimental

2.1 Copolymers

For the diblock copolymers, the polymerisation of ethylene oxide was initiated by 2-(2-methoxyethoxy)ethanol partly in the form of its potassium salt. Upon completion of this polymerisation, 1,2-butylene oxide was added and polymerised to completion. The triblock copolymer was prepared by a similar sequential copolymerisation, this time starting from 1,2-butanediol and polymerising first the butylene oxide and secondly the ethylene oxide. A brief account of the preparation of the triblock copolymer is available elsewhere,[16] and the general methods used for preparation of copolymers of both architectures have been fully described previously.[13,19]

The copolymers were characterised by gel permeation chromatography (GPC) and ^{13}C NMR spectroscopy, as described recently.[13,14] Assignments of chemical shifts for all relevant backbone, end group and junction group carbon resonances have been reported.[20] GPC, based on calibration with poly(oxyethylene) standards, was used solely to check the width of the chain length distribution, *i.e.* to determine the molar mass ratio M_w/M_n. NMR spectroscopy was used to define block lengths, making use of spectra for both precursor polymers (from the first stage of copolymerisation) and final products. Comparison of the intensities of resonances of carbons of end groups and E/B junction groups served to confirm block structure and purity. The molecular characteristics of the copolymers are given in Table 1. The wider distribution width of the triblock copolymer ($M_w/M_n = 1.1$) is as expected (see Introduction).

2.2 Surface tension

Surface tensions (γ) of dilute aqueous solutions were measured at four temperatures in the range 20–50 °C by detachment of a platinum ring using a temperature-controlled (± 0.2 °C) surface tensiometer (Kruss, Model K8600). The instrument was well protected from vibration and draughts. Copolymer solutions in deionised and doubly distilled water were made by dilution of a stock solution. A new solution was first equilibrated at the lowest temperature for 24 h and then γ was measured every 30 min until consistent readings were obtained. Thereafter, the temperature was raised and the procedure repeated. Before using a new solution the ring was washed successively with dilute HCl and water. The accuracy of measurement was checked by frequent determinations of the surface tension of pure water.

2.3 Light scattering

Glassware was washed with condensing acetone vapour before use. Solvent and solutions were clarified by filtering through Millipore Millex filters (triton free, 0.22 μm porosity, sometimes 0.1 μm porosity) directly into the cleaned scattering cell.

Static light scattering (SLS) intensities were measured by means of a Brookhaven BI-200S instrument with vertically polarised incident light of wavelength $\lambda = 488$ nm supplied by an argon–ion laser (Coherent Innova 90) operated at 500 mW. The intensity scale was calibrated against benzene. Dynamic light scattering (DLS) measurements were made under similar conditions by means of the Brookhaven instrument described above combined with a Brookhaven BI 9000 AT digital correlator. Experiment duration was in the range 5–20 min, and each experiment was repeated two or more times. In all experiments, measurement of scattered light was made at a scattering angle of 90°. The applicability of the methods to micellar solutions of the type under investigation has been discussed recently.[7,8,21]

The correlation functions from dynamic light scattering (DLS) were analysed by the constrained regularised CONTIN method[22] to obtain distributions of decay rates (Γ). The decay rates gave distributions of apparent mutual diffusion coefficient ($D_{app} = \Gamma/q'^2$, where $q' = 4\pi n \sin\theta/\lambda$, n = refractive index of the solvent, and the scattering angle is 2θ) and hence of apparent hydrodynamic radius ($r_{h,\,app}$, radius of the hydrodynamically-equivalent hard sphere corresponding to D_{app}) *via* the Stokes–Einstein equation

$$r_{h,\,app} = kT/(6\pi\eta D_{app}) \quad (1)$$

where k is the Boltzmann constant and η is the viscosity of the solvent at temperature T. In practice, intensities $I(\Gamma)$ delivered by the CONTIN program at logarithmically spaced values of decay rate were transformed to $I(\log \Gamma) = I(\Gamma)\Gamma$ to obtain intensity distributions of $\log(\Gamma)$, and so of $\log(r_{h,\,app})$. Normalisation of $I(\log r_{h,\,app})$ gave the intensity fraction distributions presented in Section 3.3.

The basis for analysis of static light scattering (SLS) was the Rayleigh–Gans–Debye equation in the form

$$I - I_s = K^* c M_w \quad (2)$$

where I is intensity of light scattered from solution relative to that from benzene, I_s is the corresponding quantity for the solvent, c is the concentration, M_w is the mass-average molar mass of the solute, and K^* is the appropriate optical constant. Values of the specific refractive index increment, its temperature increment, and other quantities necessary for the calculations, have been given previously.[13,19,21,23]

2.4 Sol/gel boundary by tube inversion

Samples of solution (0.5 g) were enclosed in small tubes (internal diameter *ca.* 10 mm), and observed whilst slowly heating (or cooling) the tube in a water bath within the range 0–85 °C. The heating/cooling rate was 0.5 °C min^{-1} or less. The change from a mobile to an immobile system (or *vice-versa*) was determined by inverting the tube. The method served to define the sol/gel transition temperatures to ± 1 °C. This simple method of detecting gelation, which is sensitive to the yield stress of the gel, has been shown to define the same hard-gel phase boundary as more sophisticated methods, *e.g.* rheometry and differential scanning calorimetry.[24]

2.5 Simultaneous SAXS/rheology

SAXS experiments were conducted at the Synchrotron Radiation Source, Daresbury Laboratory, UK, on beamline 16.1. This beamline is configured with an X-ray wavelength $\lambda = 1.5$ Å. Details of the storage ring, radiation, camera geometry and data collection electronics have been given elsewhere.[25] Scattered photons were collected on a multiwire gas-filled area detector. A scattering pattern from an oriented specimen of

Table 1 Molecular characteristics of the copolymers

Copolymer	M_w/M_n (GPC)	M_n[a]/g mol^{-1} (NMR)	E (wt.%) (NMR)	M_w[b]/g mol^{-1}
$E_{106}B_{16}$	1.03	5820	80	5990
$E_{210}B_{16}$	1.03	10400	89	10700
$E_{103}B_{15}E_{103}$	1.10	10100	89	11100

[a] M_n = number-average molar mass. [b] M_w = mass-average molar mass calculated from M_n and M_w/M_n. Estimated uncertainties: block lengths, wt.% E, M_n and M_w/M_n to 2%; M_w to 3%.

wet collagen (rat-tail tendon) was used for calibration of the q scale ($q = 4\pi\sin\theta/\lambda$, where the scattering angle is 2θ). Measurements of dynamic mechanical properties were performed, in tandem with the SAXS experiments, using a Rheometrics Solids Analyser RSA II system with a shear sandwich geometry. This instrument has been described in detail elsewhere.[26,27] Briefly, an oscillatory (sinusoidal) strain was applied and the dynamic and loss shear moduli, respectively G' and G'', were measured as a function of the deformation conditions. Apertures were machined into the plates of the shear sandwich assembly to allow transmission of the X-ray beam, and were covered by Kapton windows of 6 μm thickness. The total sample thickness was 0.5 mm. The shear sandwich was contained in an insulated oven, with temperature control to ±1 °C. With the rheometer *in situ* at the beamline, the shear direction $\boldsymbol{v}$ was vertical and the X-ray beam was incident along the horizontal shear gradient direction $\nabla\boldsymbol{v}$, the neutral direction $\boldsymbol{e} = \nabla\boldsymbol{v} \times \boldsymbol{v}$ also being horizontal. The acquisition of SAXS and rheology data was synchronised using an electronic trigger. In order to enhance contrast for separate neutron scattering experiments,[17] all solutions for SAXS/rheology were prepared using D_2O instead of H_2O.

3 Results and discussion

3.1 Clouding

Aqueous solutions of the copolymers did not cloud over the concentration and temperature ranges investigated ($c \leqslant 70$ wt.%, $T \leqslant 85$ °C).

3.2 Critical micelle concentration

Plots of surface tension against logarithm of concentration are shown in Fig. 1 for aqueous solutions of the triblock copolymer $E_{103}B_{15}E_{103}$. Corresponding plots for copolymer $E_{210}B_{16}$ have been published previously:[18] those for the other diblock copolymer were similar. Values of the critical micelle concentration (c.m.c.) derived from the intercept of the two straight lines fitting each set of data points are listed in Table 2. The larger c.m.c. of the triblock copolymer compared

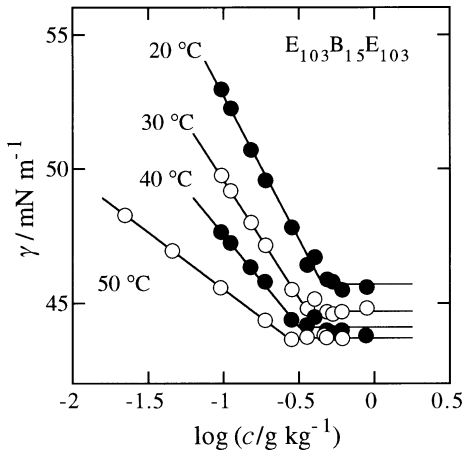

Fig. 1 Surface tension *vs.* log(concentration) for aqueous solutions of copolymer $E_{103}B_{15}E_{103}$ at the temperatures indicated.

Table 2 Critical micelle concentrations (g dm^{-3}) for aqueous solutions of E/B block copolymers[a]

Copolymer	20 °C	30 °C	40 °C	50 °C
$E_{103}B_{15}E_{103}$	0.45	0.36	0.32	0.27
$E_{106}B_{16}$	0.0047	0.0041	0.0046	0.0045
$E_{210}B_{16}$	0.0038	0.0037	0.0036	0.0042

[a] Estimated uncertainties: log(c.m.c.), ±0.1; c.m.c., ±20%.

to those of the two diblock copolymers (by a factor of 100 or so) is consistent with results from previous investigations of the effect of block architecture in the E_mB_n and $E_mB_nE_m$ systems.[5,7,13,23]

Plots of log(c.m.c.) against $1/T$ are shown in Fig. 2. The zero slopes of the plots for the two diblock copolymers indicate athermal micellisation processes (*i.e.* zero standard enthalpies of micellisation, $\Delta_{mic}H^\circ$). This unusual result has been discussed in some detail previously.[18] The small positive slope of the plot for the triblock copolymer corresponds to $\Delta_{mic}H^\circ = 14$ kJ mol^{-1}. Low values have been found for other $E_mB_nE_m$ copolymers having similar B-block lengths: *e.g.* $E_{40}B_{15}E_{40}$, $\Delta_{mic}H^\circ = 24$ kJ mol^{-1},[28] and $E_{58}B_{17}E_{58}$, $\Delta_{mic}H^\circ = 34$ kJ mol^{-1}.[29] In contrast, the standard enthalpies of micellisation of $E_mP_nE_m$ block copolymers with c.m.c.s comparable to those of $E_{103}B_{15}E_{103}$ (*i.e.* copolymers with P blocks of 50 units or more) are usually greater than 200 kJ mol^{-1}.[2] The low values of $\Delta_{mic}H^\circ$ found for the E/B copolymers, both diblock and triblock, have been explained by collapse of the B blocks of copolymers in the molecular state and, as a consequence, a small thermal effect accompanying their incorporation in the micellar core.[18,19] P units are much less hydrophobic than B units: recent measurements indicate a factor of 6.[9] Accordingly, the P blocks of copolymers in the molecular state interact more strongly with water giving rise to a larger thermal effect on micellisation.

3.3 Dynamic light scattering (DLS)

Plots of intensity fraction, $I(\log r_{h,app})$, against logarithm of apparent hydrodynamic radius, $\log(r_{h,app})$, are shown in Fig. 3 for dilute solutions (3.3–4.3 g dm^{-3}) of the three copolymers at 30 °C. The single peaks centred on $r_{h,app} = 9$–13 nm indicate micelles formed by a closed association process. The distribution found for micelles of copolymer $E_{103}B_{16}E_{103}$ is wider than those of the diblock copolymers. Results for this copolymer are presented in more detail in Fig. 4. As can be seen, the distribution width is little changed by increasing the solution concentration in the range 2.9–43 g dm^{-3} or by increasing the solution temperature from 30 to 50 °C. This insensitivity to conditions suggests that the wider micelle size distributions found for copolymer $E_{103}B_{15}E_{103}$ are caused, in part at least, by the wider chain length distribution of its E blocks (see Table 1 and related discussion), although micellar dissociation allied to the high critical micelle concentration (see Table 2) may also play a part.

In Fig. 5 the reciprocal of intensity-average apparent hydrodynamic radius (calculated in the CONTIN program by integrating over the intensity distribution of decay rate) is plotted against concentration for solutions of the three copolymers. Through eqn. (1), $1/r_{h,app}$ is proportional to $D_{app}\eta/T$, and,

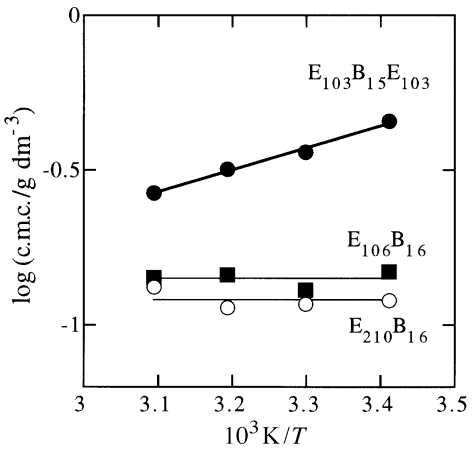

Fig. 2 Log(c.m.c.) *vs.* reciprocal temperature for aqueous solutions of the E/B block copolymers indicated.

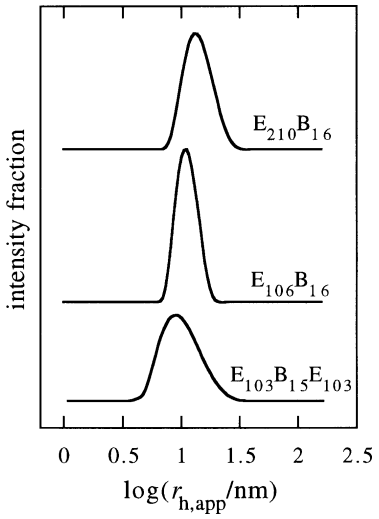

Fig. 3 Apparent hydrodynamic radius ($r_{h,app}$) from dynamic light scattering. Intensity fraction $I(\log r_{h,app})$ *vs.* $\log(r_{h,app})$ for dilute aqueous solutions of the E/B block copolymers indicated: $c = 3$–4 g dm^{-3}, $T = 30$ °C.

compared with D_{app} itself, is compensated for changes in temperature and solvent viscosity. For simplicity in the diagram, a single straight line is drawn through all the data points for a given copolymer. Actual values of r_h at zero concentration found by least-squares fitting of the individual sets of data points are listed in Table 3.

As seen in Table 3 and Fig. 5, $r_{h,app}$ is independent of temperature, within the error of determination, for micellar solutions of all three copolymers. This effect was first described some years ago for $E_mP_nE_m$ copolymers,[30] when it was attrib-

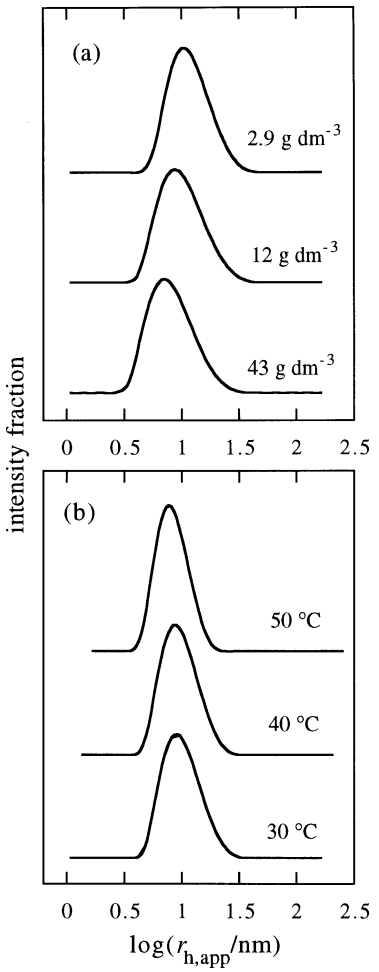

Fig. 4 Apparent hydrodynamic radius ($r_{h,app}$) from dynamic light scattering. Intensity fraction $I(\log r_{h,app})$ *vs.* $\log(r_{h,app})$ for dilute aqueous solutions of copolymer $E_{103}B_{15}E_{103}$: (a) solutions at 30 °C and the concentrations indicated; (b) 43 g dm^{-3} solution at the temperatures indicated.

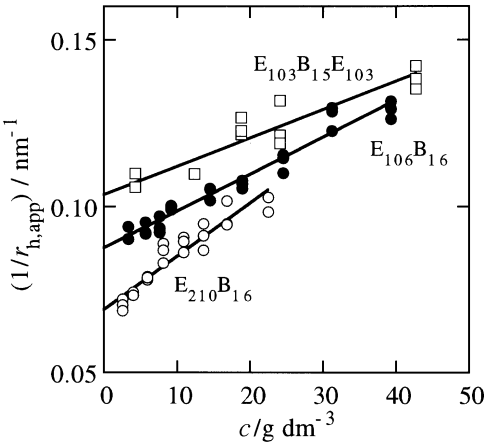

Fig. 5 Reciprocal of apparent hydrodynamic radius *vs.* copolymer concentration for solutions at 30, 40 and 50 °C of the E/B indicated. Least-squares lines are drawn through all points for a given copolymer irrespective of temperature.

Table 3 Micellar characteristics from dynamic light scattering: aqueous solutions of E/B block copolymers[a]

Copolymer	T/°C	r_h/nm	D/ 10^{-11} m^2 s^{-1}	k_d/ dm^3 g^{-1}
$E_{103}B_{15}E_{103}$	30	9.7	2.9	0.022
	40	9.2	3.8	0.026
	50	9.4	4.6	0.034
$E_{106}B_{16}$	30	11.7	2.4	0.036
	40	11.7	3.0	0.041
	50	11.1	3.9	0.041
$E_{210}B_{16}$	30	14.9	1.9	0.059
	40	14.4	2.4	0.055
	50	14.6	3.0	0.062

[a] Estimated uncertainties: r_h and D, ±4%; k_d, ±8%.

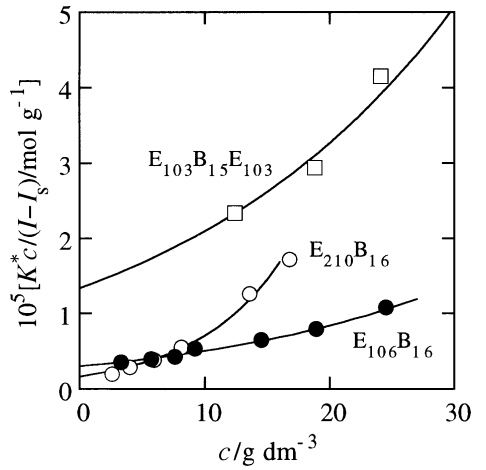

Fig. 6 Static light scattering. Scattering function *vs.* concentration for aqueous solutions of E/B block copolymers indicated. For clarity of presentation, results obtained for solutions of $E_{103}B_{15}E_{103}$ at $c > 30$ g dm^{-3} are omitted from the diagram. The curves were calculated using eqn. (6)–(8).

uted to the compensating effects of an increase in association number and a decrease in swelling of the micelle fringe as temperature was increased. Since that time there have been many confirmatory reports.[2,6]

The concentration dependence of the apparent mutual diffusion coefficient (in dilute solution) can be expressed by the equation

$$D_{app} = D(1 + k_d c) \quad (3)$$

Values of D and k_d are given in Table 3. Coefficient k_d is related to the thermodynamic second virial coefficient, A_2, through the equation[31]

$$k_d = 2A_2 M_w - k_f - 2v \quad (4)$$

where k_f is the frictional coefficient and v is the partial specific volume of the micelles in solution. In the present case it is clear that $A_2 M_w$ is large and positive for micellar solutions of all three copolymers, which is the behaviour expected for micelles acting as hard spheres. As seen in Table 3, the values of k_d increase regularly from $E_{103}B_{15}E_{103}$ to $E_{210}B_{16}$. The values of A_2 from static light scattering are consistent with this pattern (see Section 3.4).

3.4 Static light scattering (SLS)

For a non-ideal, dilute solution of particles, the Debye equation can be written

$$K^*c/(I - I_s) = 1/M_w + 2A_2 c + 3A_3 c^2 \cdots \quad (5)$$

where A_2 and A_3 are the second and third virial coefficients (higher terms being omitted). As written, the equation assumes small particles relative to the wavelength of the light. Radii of gyration, estimated (assuming uniform spheres) as *ca.* 80% of the hydrodynamic radii in Table 3, were 12 nm or less, hence any effect of destructive interference on the scattering intensity at 90 °C should be insignificant.[32]

Eqn. (5) is commonly used truncated to the second term to produce a straight line plot. Its use in this form is not satisfactory for the present systems. This is because micellar interaction at moderate concentrations causes curvature of the Debye plot across any significant concentration range. This feature is illustrated in Fig. 6 in which the $K^*c/(I - I_s)$ is plotted against concentration for the three copolymers in water at 30 °C. A similar plot for solutions of copolymer $E_{210}B_{16}$ at the three temperatures studied has been published previously.[18] Curvature in the plot was particularly pronounced for micellar solutions of copolymer $E_{210}B_{16}$, but was also important for solutions of copolymer $E_{103}B_{15}E_{103}$ which has a relatively high c.m.c. making it necessary to work at concentrations above 10 g dm^{-3} in order to avoid micellar dissociation.

Extrapolation of the curved plots to zero concentration was guided by the theoretical expression for scattering from hard spheres,[33] making use of the Carnahan–Starling equation,[34] which is equivalent to the virial expansion for the structure factor taken to its seventh term. Consideration was given to fitting the data using the expression for hard spheres with two virial coefficients or, more arbitrarily, by a linear plot of the square-root of $K^*c/(I - I_s)$ against concentration. The Carnahan–Starling equation gave the most satisfactory results across the three systems and, since it provided a consistent treatment with just two adjustable parameters, was adopted. In the procedure, the interparticle interference factor (structure factor, S) in the scattering equation

$$K^*c/(I - I_s) = 1/SM_w \quad (6)$$

is approximated by

$$1/S = [(1 + 2\phi)^2 - \phi^2(4\phi - \phi^2)](1 - \phi)^{-4} \quad (7)$$

where ϕ is the volume fraction of equivalent uniform spheres. Values of ϕ were calculated from the volume fraction of micelles in the system by applying a thermodynamic expansion factor δ_t, *i.e.* the ratio of the thermodynamic volume (v_t, one-eighth of the excluded volume) to the anhydrous volume (v_a):

$$\delta_t = \frac{v_t}{v_a} \quad (8)$$

Concentrations were converted to volume fractions using densities of anhydrous polymer (ρ_a) in the range 1.10–1.08 g cm^{-3} according to temperature.[35] The curves drawn in Fig. 6 were obtained in this way, that for copolymer $E_{103}B_{15}E_{103}$ including data obtained at higher concentrations than shown. Similar treatment of all results gave the values of the two adjustable parameters (M_w and δ_t) listed in Table 4, together with association numbers of the micelles calculated from:

$$N_w = M_w(\text{micelle})/M_w(\text{molecule}) \quad (9)$$

using the values of M_w(molecule) listed in Table 1. Also listed in Table 4 are values of the equivalent hard-sphere radius (thermodynamic radius, r_t) calculated from the thermodynamic volume (*i.e.* from $v_t = \delta_t v_a$).

3.5 Sol/gel boundary

Sol/gel boundaries in the concentration range 5–25 wt.% and temperature range 0–80 °C determined by tube inversion are shown in Fig. 7. The intention was to define critical gel concentrations (c.g.c.) for the three copolymers. As is evident from Fig. 7, at any given temperature the c.g.c.s lie in the order $E_{210}B_{16} < E_{106}B_{16} < E_{103}B_{15}E_{103}$.

As shown in Section 3.6, SAXS patterns indicate that all the gels studied had body-centred cubic (bcc) structures, presumably based on packed spherical micelles. Previously, we have shown that the expansion factor deduced from light scattering studies of micelles in dilute solution (δ_t of Table 4) may serve

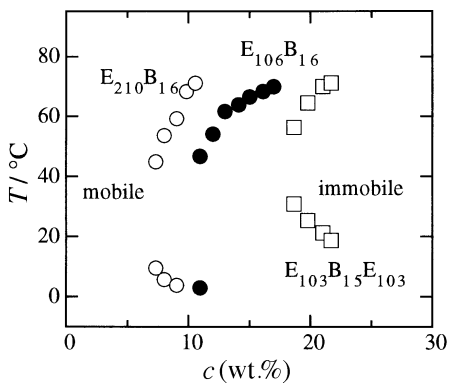

Fig. 7 Phase (sol/gel) diagram for aqueous solutions of the E/B block copolymers indicated.

Table 4 Micellar characteristics from static light scattering: aqueous solutions of E/B block copolymers[a]

Copolymer	T/°C	M_w/ 10^5 g mol^{-1}	N_w	δ_t	r_t/ nm
$E_{103}B_{15}E_{103}$	30	0.75	7	6.3	5.5
	40	1.05	10	6.4	6.3
	50	1.4	13	6.5	6.9
$E_{106}B_{16}$	30	3.3	55	7.2	9.5
	40	3.9	65	7.3	10.2
	50	4.4	73	7.3	10.6
$E_{210}B_{16}$	30	6.0	56	20	16
	40	7.1	66	19	17
	50	8.7	81	18	18

[a] Estimated uncertainties: M_w, N_w to ±15%, r_t to ±10%, d_t to ±5%.

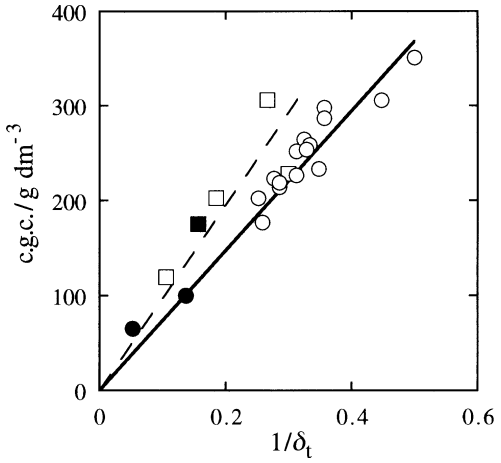

Fig. 8 Critical gel concentration *vs.* reciprocal of the thermodynamic expansion factor for micelles of E/B copolymers in aqueous solution. Squares denote $E_mB_nE_m$ copolymers and circles denote E_mB_n copolymers. Data points for the present copolymers are shown as filled symbols.

as a useful predictor of the c.g.c. of solutions of diblock copolymers.[15,36] In this respect δ_t relates to the ratio r_t^3/M_w and is sensitive to total excluded volume rather than to the micellar size itself.[19,28,29,36,37] For a bcc structure formed from spheres, the critical condition for gel formation is reached when the volume fraction of spheres in the system (ϕ) reaches a value of 0.68. Using δ_t, the critical copolymer concentration for gelation in g dm^{-3} is given by

$$\text{c.g.c.} = 10^3 \phi_c \rho_a / \delta_t \quad (10)$$

where ρ_a is the density of the liquid copolymer. The values of δ_t for solutions at 40 °C (taken from Table 4), used in eqn. (10), lead to the values of the c.g.c. at 40 °C listed in Table 5, where they are converted to wt.% copolymer. Comparison is made with experimental values taken from Fig. 7. The prediction is good for solutions of $E_{106}B_{16}$ but poor for solutions of the other two copolymers. Poor prediction *via* eqn. (10) of the c.g.c. for solutions of triblock $E_mB_nE_m$ copolymers has been noted previously.[15] A plot of the c.g.c. (g dm^{-3}) against $1/\delta_t$ including present and previous results (see Fig. 8) shows that the c.g.c. found for $E_{103}B_{15}E_{103}$ is consistent with other results for triblock copolymers. The dashed curve drawn on Fig. 8, which is a rough fit to the data points for the triblock copolymers, corresponds to $\phi_c = 0.9$, the value expected for cylinders. However, there is no evidence from SAXS to suggest structures of hexagonally packed cylinders (see Section 3.6), and examination of the gels by polarised-light microscopy showed no birefringence. The poor prediction of the c.g.c. for solutions of $E_{210}B_{16}$ may well reflect an impropriety in fitting eqn. (6) and (7) to intensities of light scattered from highly expanded micelles.

Table 5 Predicted and found critical gel concentrations for aqueous solutions at 40 °C of E/B copolymers

Copolymer	δ_t[a]	c.g.c.(wt.%) (predicted)	c.g.c.(wt.%) (found)
$E_{103}B_{15}E_{103}$	6.4	116	175
$E_{106}B_{16}$	7.3	101	100
$E_{210}B_{16}$	19	39	65

[a] Results for δ_t from Table 4.

3.6 SAXS and rheology

Gels of the three copolymers in D_2O (concentrations 30 and 45 wt.%) were held at 25 °C and examined by SAXS. The 30 wt.% $E_{106}B_{16}$ gel was also examined at temperatures up to 75 °C. All were found to have scattering patterns consistent with body-centred cubic structures (bcc). The results described below are mainly those obtained for the 30 wt.% gels.

Representative SAXS profiles for the 30 wt.% gels are shown in Fig. 9. These profiles were obtained by radial integration of two-dimensional patterns obtained for samples as mounted (*i.e.* without deliberate orientation) in the SAXS rheometer at 25 °C. They indicate structures of probable bcc (space group $Im\bar{3}m$) symmetry for which the sequence of allowed reflections is 110, 200, 211, 220, 310.., producing

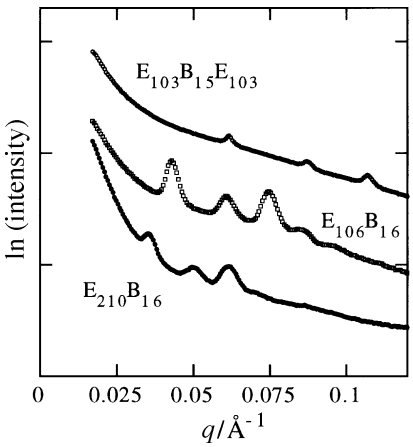

Fig. 9 SAXS profiles measured at 25 °C for aqueous gels containing 30 wt.% copolymer. Top: $E_{103}B_{15}E_{103}$, middle: $E_{106}B_{16}$, bottom: $E_{210}B_{16}$ (as indicated). For clarity, successive curves are offset vertically.

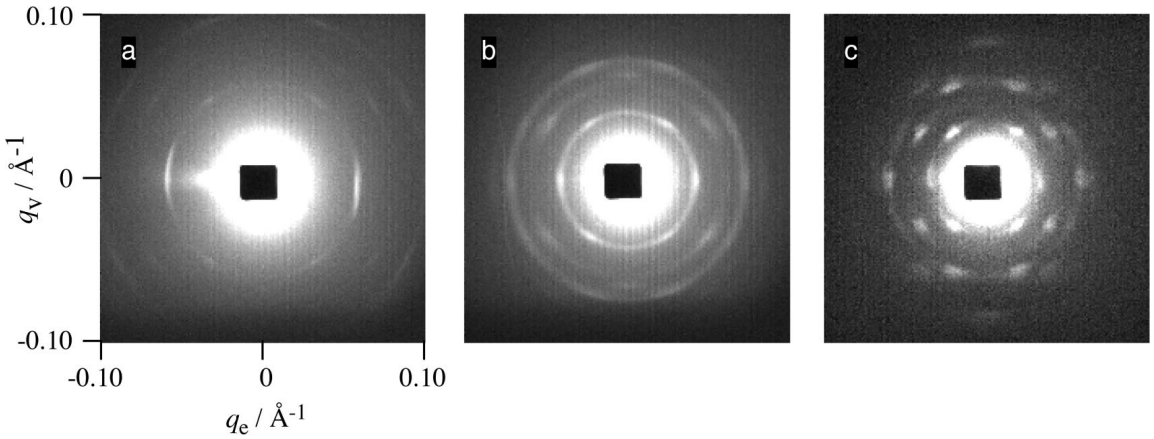

Fig. 10 SAXS patterns recorded at 25 °C for aqueous gels containing 30 wt.% copolymer, following oscillatory shear at frequency $\omega = 100$ rad s^{-1} and strain amplitude $A = 100\%$. (a) $E_{103}B_{15}E_{103}$, (b) $E_{106}B_{16}$, (c) $E_{210}B_{16}$. The shear direction is vertical.

peaks in the positional ratio 1: $\sqrt{2}$:$\sqrt{3}$:2:$\sqrt{5}$. The first five orders of reflection are visible for the $E_{106}B_{16}$ gel, but only the first three orders for the other two copolymers. Lattice parameters for the bcc unit cells were obtained by plotting peak position (q) *versus* $(h^2 + k^2 + l^2)^{1/2}$ where h, k, l label the Miller indices. The resulting values (parameter a in Table 6) reveal, as might be expected, a correlation between lattice parameter and E-block length, values for both quantities being in the sequence $E_{210}B_{16} > E_{106}B_{16} > E_{103}B_{15}E_{103}$.

Also listed in Table 6 are the effective radii (r_x) of the micelles in the bcc unit cells of the 30 wt.% gels at 25 °C, as calculated from the lattice parameters assuming $\phi = 0.68$ and two micelles per unit cell. These can be compared with the corresponding values of the thermodynamic radius at 25 °C: the values in Table 6 were obtained by extrapolation of those in Table 4. The thermodynamic radius relates directly to the exclusion effect, and is the effective collision radius of spherical micelles at infinite dilution. Excepting copolymer $E_{210}B_{16}$, for which there are doubts about the accuracy of r_t (see Section 3.4) the approximate agreement between r_t and r_x indicates that the micelles are effectively unchanged in their exclusion properties between dilute solution and gel phases. This constancy has been noted previously by Mortensen and coworkers for aqueous solution and gels of $E_mP_nE_m$ copolymers investigated by SANS.[38,39]

The scattering patterns from the 30 wt.% gels of all three copolymers were qualitatively similar over the temperature range 25–75 °C. Those for copolymer $E_{106}B_{16}$ were analysed in some detail and values of q^* were found to scatter around a mean value of 0.044 ± 0.003 Å^{-1}, leading to $r_x = 88 \pm 6$ Å. Because of the scatter, it was not possible to define closely the temperature dependence of r_x. Considering further the 30 wt.% $E_{106}B_{16}$ gel, and using an approximate gel density of 1.10 g cm^{-3} (solution in D_2O) the mass of solution per unit cell is 9.1×10^{-18} g, hence the mass of copolymer per micelle (2 micelles per unit cell) is 1.4×10^{-18} g, corresponding to a micellar molar mass of 8.5×10^6 g mol^{-1}, *i.e.* an association number about twice that in dilute solution (see Table 4). A larger increase in micellar molar mass on passing from the dilute solution to the gel state was found previously for copolymer $E_{86}B_{10}$ in salt solution,[40] but in that case r_x was significantly larger than r_t.

Further confirmation of a bcc structure was provided by shear orientation of the 30 wt.% gel using large amplitude oscillatory shear. Simultaneous SAXS/rheology experiments were conducted during this process. The SAXS patterns shown in Fig. 10 were obtained for gels held at 25 °C following shear at frequency $\omega = 100$ rad s^{-1} and strain amplitude $A = 100\%$ for at least 5 min (*i.e. ca.* 5000 cycles of shear). The patterns indicate a susceptibility to shear in the order $E_{210}B_{16} > E_{106}B_{16} > E_{103}B_{15}E_{103}$, which may reflect the extent of gelation, *i.e.* distance from the gel/sol boundary (see Fig. 7). However, there is no corresponding trend in gel stiffness (quantified through the isothermal/isochronal dynamic elastic shear modulus, G') to support this conjecture. Irrespective of the extent of alignment, the symmetry of all three patterns in Fig. 10 is similar. In fact, patterns of this symmetry have previously been identified by our group *via*

Table 6 Lattice parameters and micellar radii for bcc aqueous gels of E/B copolymers at 25 °C

Copolymer	a^a/nm	$r_x{}^a$/nm	$r_t{}^b$/nm
$E_{103}B_{15}E_{103}$	14.4	6.2	5
$E_{106}B_{16}$	21.1	9.3	9
$E_{210}B_{16}$	24.4	10.6	15

[a] Estimated uncertainty: a, ±7%; r_x, ±9%. [b] Results for r_t by extrapolation of data in Table 4.

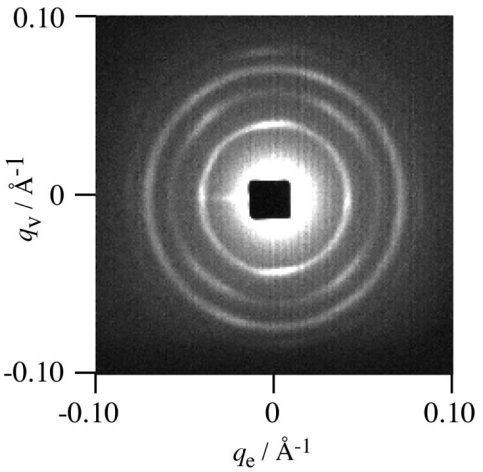

Fig. 11 SAXS pattern obtained for a 30 wt.% $E_{106}B_{16}$ aqueous gel. The sample was as mounted in the rheometer at 25 °C prior to the application of oscillatory shear. The shear direction is vertical.

SAXS/rheology or SANS/rheology experiments on bcc gels of E_mB_n diblock copolymers in aqueous solutions.[27,41,42] They are characterised by six inner 110 reflections, with two on the equator and four at ±55° with respect to the equator. The data for $E_{106}B_{16}$ and $E_{210}B_{16}$ also reveal four 200 reflections at ±35° with respect to the equator and for the latter copolymer, higher order reflections, including ten 211 reflections, with a characteristic distribution of orientations. As described elsewhere,[27,41,42] these patterns can be indexed to a highly twinned bcc structure in which a [111] direction of the bcc lattice lies along the shear direction, and flow is in the {110}, {211} and {321} planes which intersect along a common [111] direction. The equatorial 110 reflections in the pattern for $E_{103}B_{15}E_{103}$ are much more intense than the other four, and this shows that flow in this gel occurs primarily in the $\{211\}\langle 111\rangle$ slip system, as described previously.[41] The off-equatorial reflections have a comparable intensity to the equatorial ones for the other two copolymers, showing that flow in {110} and {321} planes is comparably active.

We have previously reported results from a study of a 40 wt.% aqueous gel of $E_{210}B_{16}$ in which SANS was in tandem with rheology (using a rheometer identical to that used for the SAXS/rheology work described here).[17] Those measurements exploited a goniometer to probe the crystallography of the gel aligned by large amplitude oscillatory shear, and thus provided information on the three-dimensional orientation of the bcc structure. That work revealed an orientation of the bcc structure that was subtly different from that which produced the SAXS patterns in Fig. 10. The equatorial 110 reflections were absent in the (*v*,*e*) plane; instead they were observed following 30° rotation around the shear axis.[17] Furthermore, the patterns were recovered on rotation through integer multiples of 60°, revealing a six fold symmetry around the shear direction. These results also indicated an aligned structure in which a [111] direction was along the shear direction, and flow was in (110)-type planes. However there was only a single twinning plane, perpendicular to the (110)-type planes, the twins being oriented at ±35.3° with respect to the shear direction. In contrast, the SAXS results for the 30 wt.% gel of the same copolymer (described above) show that flow is activated in {211} and {321} planes as well. The origin of this difference in flow behaviour is at present unclear. Concentration difference can be ruled out, because SAXS/rheology experiments on a 45 wt.% gel (data not illustrated) revealed a pattern similar to that shown in Fig. 10(c). One possible cause is the higher strain amplitude ($A = 150\%$) employed in the SANS/rheology measurements. A second is differences in the shear sandwich configuration in the two experiments: in particular, in the SANS rheometer the sample gap was 0.3 mm and the tools

were made of aluminium, whereas in the SAXS rheometer the sample gap was 0.5 mm and the gel was in contact with Kapton. These distinct boundary conditions could lead to different flow mechanisms.

A different projection of the cubic structure (providing further strong evidence for a bcc phase) was noted for several samples after mounting in the rheometer, a process which involved some compression between the plates of the shear sandwich. A representative SAXS pattern for an 'as mounted' 30 wt.% $E_{106}B_{16}$ gel is shown in Fig. 11. This reveals a four-fold symmetry of 110 and 200 reflections, with 110 reflections on the equator (predominant) and meridian. A similar pattern has been observed for bcc gels of copolymer $E_{40}B_{10}$ in aqueous salt solution. It results from an aligned structure in which 110 planes are both parallel and perpendicular to ($\boldsymbol{v}$,$\nabla\boldsymbol{v}$) plane.[43,44] This orientation is not observed for samples subject to oscillatory shear because the majority of 110 planes would be orthogonal to the shear direction, a so-called "forbidden" orientation.

Values of the elastic (G') and loss (G'') dynamic moduli obtained during an isochronal temperature ramp for a 30 wt.% gel of $E_{106}B_{16}$ are shown in Fig. 12. The value of G' indicates a hard gel, based on the empirical definition $G' > 10^4$ Pa.[24,45,46] The hard gel is stable up to at least 75 °C (the temperature was not increased further due to problems with solvent loss). Similar results were obtained for 30 wt.% gels of the other two copolymers, *i.e.* $G' > 10^5$ Pa, and an upper boundary above 75 °C (consistent with the phase diagram shown in Fig. 7).

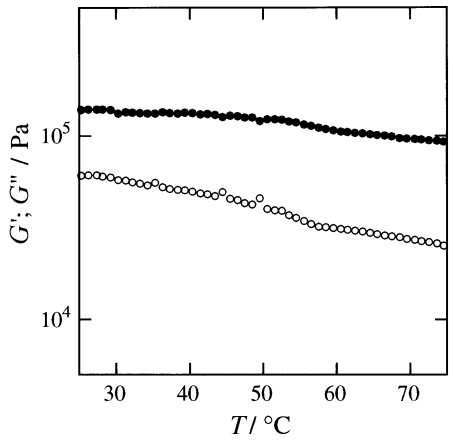

Fig. 12 Temperature dependence of (●) elastic modulus G' and (○) loss modulus G'' for a 30 wt.% $E_{106}B_{16}$ aqueous gel sheared at frequency $\omega = 10$ rad s^{-1} and strain amplitude $A = 1\%$. The heating rate was 2 °C min^{-1}.

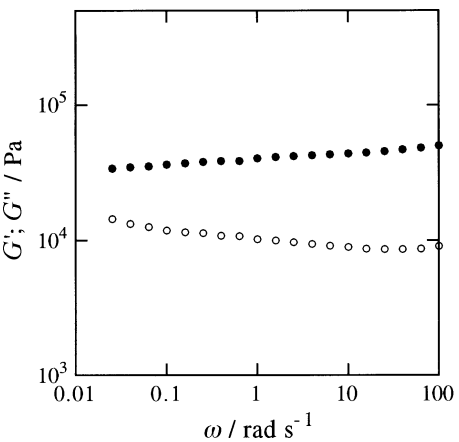

Fig. 13 Frequency dependence of (●) elastic modulus G' and (○) loss modulus G'' for a 30 wt.% $E_{210}B_{16}$ aqueous gel at 25 °C sheared at strain amplitude $A = 1\%$.

Fig. 12 contains evidence for a weak transition near 55 °C. This effect was most pronounced for the $E_{103}B_{15}E_{103}$ gels. It is tempting to ascribe the effect to a departure of the constituent micelles from spherical towards cylindrical symmetry, since this would reduce the packing constraints and so lower the elastic modulus. In this respect, the eventual formation of cylindrical micelles at high temperatures in concentrated aqueous solutions of E/B and E/P block copolymer micelles is not in doubt.[26,38,39,47] However, no qualitative changes in scattering pattern were observed within the temperature range explored by SAXS (25–75 °C).

As expected for a cubic phase, the low frequency viscoelastic response is only weakly dependent on frequency,[48] as illustrated by the representative results for a 30 wt.% $E_{210}B_{16}$ gel at 25 °C shown in Fig. 13.

4 Concluding remarks

A range of techniques have been used to improve our understanding of the effect of block architecture on the self-association of a block-copolymer across a wide concentration range: surface tensiometry for critical micelle concentration and its temperature dependence, light scattering for micelle association number and radius, and X-ray scattering and rheometry for gel structure and modulus. The whole project was underpinned by the controlled synthesis and characterisation of the block copolymers.

Exploration of the effect of block architecture on the micellisation of block copolyethers in aqueous solution relates directly to the dominance of the triblock architecture in the commercial field, *e.g.* of the Pluronic and Synperonic-PE copolymers of type $E_mP_nE_m$ produced by BASF and ICI C&P, respectively, and to a lesser extent of the $E_mB_nE_m$ copolymers produced by the Dow Chemical Co. In keeping with a number of recent reports, referred to above, the present results confirm that diblock copolymers micellise more readily than their triblock counterparts and, in particular, show that this effect extends unchanged to copolymers with lengthy E blocks. While micellisation is neither necessary nor desirable for many applications of block copolyethers in aqueous systems, there are some applications in which it is all important. One such application is the solubilisation of sparingly soluble drugs, and it is clear that in this area diblock copolymers have the advantage over triblock copolymers. At room temperature, the diblock copolymers of present interest micellise at one-hundredth the concentration of that necessary for micellisation of the triblock copolymer: see Table 2. Unusually, the critical micelle concentrations of the diblock copolymer were found to be independent of temperature: see Fig. 2.

In more concentrated systems, the molecule–micelle equilibrium overwhelmingly favours micelles, and solution properties are determined by the size and shape of the micelles. However these micellar properties reflect the architecture of the underlying block copolymers. A property of considerable interest is the formation of aqueous gels, and particularly the high-modulus (hard) gels which result from cubic packing of spherical micelles. Such gels, complete with solubilised drug, have potential for controlled release without the need for surgical implantation and eventual removal. All three copolymers investigated in this work formed hard gels with body-centred cubic packing, but inspection of Fig. 7 shows clearly the advantage of the diblock architecture for the formation of hard gels at relatively modest concentrations (10 wt.% or less in the present case). Our results confirm that swelling of the micelle fringe (quantified in favourable cases through the thermodynamic expansion factor, δ_t) is the important determinant of the critical concentration of copolymer for formation of hard gel. Underlying this effect is the observation that micelles

in the gel state have similar radii but larger association numbers than those in dilute solution.

Acknowledgements

We are grateful to the EPSRC for a grant (GR/K56117) from the Soft Solids Processing Initiative that supported the SAXS/rheology work, and to A. J. Gleeson (Daresbury Lab) for assistance with the SAXS experiments. Copolymer synthesis was supported by EPSRC grant GR/J25904. L.D. was in receipt of an EPSRC Research Studentship.

References

1 I. R. Schmolka in *Nonionic Surfactants*, *Surfactant Science Series*, ed. M. J. Schick, Marcel Dekker, New York, 1967, vol. 1, ch. 10.
2 B. Chu and Z-K. Zhou in *Nonionic Surfactants: Polyoxyalkylene Block Copolymers*, ed. V. M. Nace, Marcel Dekker Inc., New York, 1996, ch. 3.
3 K. Mortensen, *J. Phys. Condens. Matter*, 1996, **8**, A103.
4 *Technical Literature*, *B-Series Polyglycols. Butylene Oxide/Ethylene Oxide Block Copolymers*, The Dow Chemical Co., Freeport, Texas, 1994.
5 V. M. Nace, *J. Am. Oil Chem. Soc.*, 1996, **73**, 1.
6 C. Booth, G-E. Yu and V. M. Nace in *Amphiphilic Block Copolymers. Self-assembly and Applications*, ed. P. Alexandridis and B. Lindman, Elsevier, Amsterdam, in the press.
7 Y-W. Yang, N-J. Deng, G-E. Yu, Z-K. Zhou, D. Attwood and C. Booth, *Langmuir*, 1995, **11**, 4703.
8 Y-W. Yang, Z. Yang, Z-K. Zhou, D. Attwood and C. Booth, *Macromolecules*, 1996, **29**, 670.
9 H. Altinok, S. K. Nixon, P. A. Gorry, D. Attwood, C. Booth, A. Kelarakis and V. Havredaki, *Colloids Surf. B*, in the press.
10 G-E. Yu, A. J. Masters, F. Heatley, C. Booth and T. G. Blease, *Macromol. Chem. Phys.*, 1994, **195**, 1517.
11 V. M. Nace, R. H. Whitmarsh, M. W. Edens, *J. Am. Oil Chem. Soc.*, 1994, **71**, 777.
12 G-E. Yu, Z. Yang, M. Ameri, D. Attwood, J. H. Collett, C. Price and C. Booth, *J. Phys. Chem., B*, 1997, **101**, 4394.
13 Z. Yang, S. Pickard, N-J. Deng, R. J. Barlow, D. Attwood and C. Booth, *Macromolecules*, 1994, **27**, 2371.
14 G-E. Yu, Z. Yang, D. Attwood, C. Price and C. Booth, *Macromolecules*, 1996, **29**, 8479.
15 Y-W. Yang, Z. Ali-Adib, N. B. McKeown, A. J. Ryan, D. Attwood and C. Booth, *Langmuir*, 1997, **13**, 1860.
16 P. C. Griffiths, T. Cosgrove, J. Shar, S. M. King, G-E. Yu, C. Booth and M. Malmsten, *Langmuir*, 1998, **14**, 1799.
17 I. W. Hamley, K. Mortensen, G-E. Yu and C. Booth, *Macromolecules*, 1998, **31**, 6958.
18 A. Kelarakis, V. Havredaki, G-E. Yu, L. Derici and C. Booth, *Macromolecules*, 1998, **31**, 944.
19 A. D. Bedells, R. M. Arafeh, Z. Yang, D. Attwood, F. Heatley, J. C. Padget, C. Price and C. Booth, *J. Chem. Soc., Faraday Trans.*, 1993, **89**, 1235.
20 F. Heatley, G-E. Yu, W-B. Sun. E. J. Pywell, R. H. Mobbs and C. Booth *Eur. Polym. J.*, 1990, **26**, 583.
21 Z. Yang, Y-W. Yang, Z-K. Zhou, D. Attwood and C. Booth, *J. Chem. Soc., Faraday Trans.*, 1996, **92**, 257.
22 S. W. Provencher, *Makromol. Chem.*, 1979, **180**, 201.
23 G-E. Yu, Y-W. Yang, Z. Yang, D. Attwood, C. Booth and V. M. Nace, *Langmuir*, 1996, **12**, 3404.
24 H. Li, G-E. Yu, C. Price, C. Booth, E. Hecht and H. Hoffmann, *Macromolecules*, 1997, **30**, 1347.
25 N. Bliss, J. Bordas, B. D. Fell, N. W. Harris, W. I. Helsby, G. R. Mant, W. R. Smith, and E. Towns-Andrews, *Rev. Sci. Instrum.*, 1995, **66**, 1311.
26 J. A. Pople, I. W. Hamley, J. P. A. Fairclough, A. J. Ryan, G-E. Yu and C. Booth, *Macromolecules*, 1997, **30**, 5721.
27 I. W. Hamley and J. A. Pople, *J. Appl. Cryst.*, in the press.
28 Y-Z. Luo, C. V. Nicholas, D. Attwood, J. H. Collett, C. Price and C. Booth, *Colloid Polym. Sci.*, 1992, **270**, 1094.
29 Y-Z. Luo, C. V. Nicholas, D. Attwood, J. H. Collett, C. Price, C. Booth, B. Chu and Z-K. Zhou, *J. Chem. Soc., Faraday Trans.*, 1993, **89**, 539.
30 D. Attwood, J. H. Collett and C. J. Tait, *Int. J. Pharm.*, 1985, **26**, 25.
31 J. Selser in *Light Scattering, Principles and Development*; ed. W. Brown, Clarendon Press, Oxford, 1996, p. 237; H. Vink, *J. Chem. Soc., Faraday Trans. 1*, 1985, **81**, 1725.
32 E. F. Casassa in *Polymer Handbook*, ed. J. Brandrup and E. H. Immergut, 3rd edn., Wiley, New York, 1989, p. 485; W. H. Beattie and C. Booth, *J. Phys. Chem.*, 1960, **64**, 696.
33 A. Vrij, *J. Chem. Phys.*, 1978, **69**, 1742.
34 N. F. Carnahan and K. E. Starling, *J. Chem. Phys.*, 1969, **51**, 635.
35 S-M. Mai, C. Booth and V. M. Nace, *Eur. Polym. J.*, 1997, **33**, 991.
36 N-J. Deng, Y-Z. Luo, S. Tanodekaew, N. Bingham, D. Attwood and C. Booth, *J. Polym. Sci., Part B, Polym. Phys.*, 1995, **33**, 10.
37 A. D. Bedells, R. M. Arafeh, Z. Yang, D. Attwood, J. C. Padget, C. Price and C. Booth, *J. Chem. Soc., Faraday Trans.*, 1993, **89**, 1243; S. Tanodekaew, N-J. Deng, S. Smith, Y-W. Yang, D. Attwood and C. Booth, *J. Phys. Chem.*, 1993, **97**, 11847.
38 K. Mortensen and J. S. Pedersen, *Macromolecules*, 1993, **26**, 805.
39 K. Mortensen W. Brown and W. Norden, *Phys. Rev. Lett.*, 1992, **68**, 2340.
40 I. W. Hamley, C. Booth, L. Derici, M. Impéror-Clerc and P. Davidson, *Phys. Rev. E*, in the press.
41 I. W. Hamley, J. A. Pople, J. P. A. Fairclough, A. J. Ryan, C. Booth and Y-W. Yang, *Macromolecules*, 1998, **31**, 3906.
42 I. W. Hamley, J. A. Pople, C. Booth, Y-W. Yang and S. M. King, *Langmuir*, 1998, **14**, 3182.
43 I. W. Hamley, J. A. Pople, J. P. A. Fairclough, N. J. Terrill, A. J. Ryan, C. Booth, G-E. Yu, O. Diat, K. Almdal, K. Mortensen and M. Vigild, *J. Chem. Phys.*, 1998, **108**, 6929.
44 I. W. Hamley, J. A. Pople and O. Diat, *Colloid Polym. Sci.*, 1998, **276**, 446.
45 M. Almgren, W. Brown and S. Hvidt, *Colloid Polym. Sci.*, 1995, **273**, 2.
46 S. Hvidt, E. Jorgensen, W. Brown and K. Schillen, *J. Phys. Chem.*, 1994, **98**, 12320.
47 O. Glatter, O. Scherf, K. Schillen and W. Brown, *Macromolecules*, 1994, **27**, 805.
48 M. Portmann, E. H. Landau and P. L. Luisi, *J. Phys. Chem.*, 1991, **95**, 8437.

Paper 8/07460G